J. Fluid Mech. (1972), *vol.* 51, *part* 1, *pp.* 159–175
Printed in Great Britain

An experimental and theoretical study of internal waves generated by the collapse of a two-dimensional mixed region in a density gradient

By A. H. SCHOOLEY
Naval Research Laboratory, Washington, D.C.
AND B. A. HUGHES
Defence Research Establishment Pacific, Forces Mail Office, Victoria, B.C., Canada

(Received 14 September 1970 and in revised form 2 August 1971)

Previously reported experiments with a self-propelled body submerged in a fluid with a stable vertical density gradient have demonstrated that the turbulently mixed wake first expands more or less uniformly and then collapses vertically while continuing to expand horizontally (Schooley & Stewart 1963). It was also shown that the vertical collapse of the wake generates internal waves. Essentially two-dimensional experiments have also been used to explore some of the build-up and decay characteristics of vertical wake collapse induced by a submerged burst of turbulent mixing (Wu 1969; Schooley 1968). The present paper reports new experimental measurements and a linear theoretical analysis of the internal wave field created in stratified water by a burst of submerged turbulent mixing. The forcing function has been obtained in integral form for an initial-value model of wake collapse in terms of a general Brunt–Väisälä frequency profile, using normal mode theory. Numerical results have been determined for the specialized case of a completely mixed circular wake in a constant Brunt–Väisälä profile. These results are compared to the experimental measurements.

1. Introduction

The concept of internal wave generation by collapse of a region of density stratified fluid which has been mixed has existed for many years and various researchers have contributed to the experimental, theoretical or to both sides of the problem. Schooley & Stewart (1963) measured the initial phase of collapse in the wake of a self-propelled body and demonstrated that wave-like effects appeared at the surface. Furthermore, they convincingly showed that the general characteristics of the surface phenomena can be explained by the existence of a number of modes of internal waves generated by the wake collapse. Their analysis, however, was not aimed at predicting the amplitude of the internal wave motion from features of the initial mixed region. Stockhausen, Clark & Kennedy (1966) also made observations relating to wake collapse behind a self-propelled body. They were concerned chiefly with the shape of the wake during the initial expansion and subsequent collapse and did not analyse their results from the

point of view of internal wave generation. Observations on the details of a mixed region during collapse in a two-dimensional laboratory model were also taken by Wu (1969). The mixed region in this case was formed by stirring a contained semi-cylindrical region at one end wall of a tank containing stratified fluid. The collapse was simulated by quickly and smoothly removing the containing apparatus and allowing the mixed fluid to flow into the stratified fluid. Very detailed results were obtained showing the subsequent shape of the mixed region. The internal wave patterns associated with the collapse were also determined and results giving the phase configuration were obtained. No amplitude information was illustrated; however, it was observed that wave heights as large as 0·2 of the mixed region radius were formed.

A wide range of theoretical results have been obtained concerning internal waves in general. Most results have been obtained for linear models. A very comprehensive treatment of the problem (for general transient or steady generation) is given by Lighthill (1967) and further detailed theoretical work with careful experimental verification is given in Mowbray & Rarity (1967). The former is concerned with a general treatise of dispersive waves in homogeneous media and one section deals specifically with internal waves generated behind a vertically moving steady disturbance. Experimental verification of the phase configuration is provided. The latter publication provides a complete linear theoretical treatment for forced internal waves in a (predominantly) homogeneous medium and deals at some length with the asymptotic solution of the Cauchy–Poisson problem. The observational data provided confirms the theoretical predictions regarding phase configurations. No comparison of amplitudes was undertaken. Impulsively generated internal waves in the atmosphere have been studied quite intensively (Pierce & Posey 1970) but not from the point of view of generation by wake collapse. Very recently, a linear theoretical analysis has been performed on wave generation by wake collapse (and other causes) by Miles (1970). A non-linear numerical analysis of the problem has been undertaken by Wessel (1969) with a comparison to the experimental results of Wu (1969).

The purpose of the present paper is to outline further experimental results concerning waves generated by mixed region collapse and to present a comparative theoretical analysis, including prediction of amplitudes using a very simple, highly idealized linear model. The experiments were performed in a small laboratory tank in which a density gradient was created by maintaining a vertical temperature gradient in water and the mixed region was formed by rapidly stirring a small part of the fluid. The internal waves were measured by a thermistor placed near one wall of the tank. Results from four density profiles are illustrated. The theoretical model is based on the theory of linear modes and is used to predict the subsequent motion due to the internal waves (amplitude and phase) in terms of the maximum turbulent expansion of the mixed region. The forcing function in this case is composed of the initial buoyancy defect moments in the mixed region and is calculated following a scheme originally proposed by Lighthill (1964, private communication). Viscous effects are included.

Since linearized internal wave models are readily amenable to mathematical treatment it is believed that this comparison of theory and experiment is doubly

valuable – it not only provides a background on which to understand the experimental results but also provides a useful indication of how detailed a mathematical model is needed in order to make useful quantitative predictions of resulting wave fields.

2. Discussion of experimental conditions and results

Figure 1 (plate 1) is a picture of the 'two-dimensional' transparent cell that was used, with dimensions 30 cm wide, 7·3 cm deep and 2·5 cm thick and grid lines 2 cm apart. For the experiments the cell was completely filled with distilled water between the bottom and top copper strips. Stable stratification of the water (more dense below than above) was produced by cooling the lower copper strip and heating the upper one. The amount of cooling and heating was controlled by the polarity and amount of electrical direct current applied to commercial thermo-electric units (modern Peltier effect devices) attached to the copper strips. For efficient and stable operation the unattached surfaces of the 1·1 cm thick thermo-electric devices were held at a constant temperature by circulating water through jackets as shown in the upper part of figure 1.

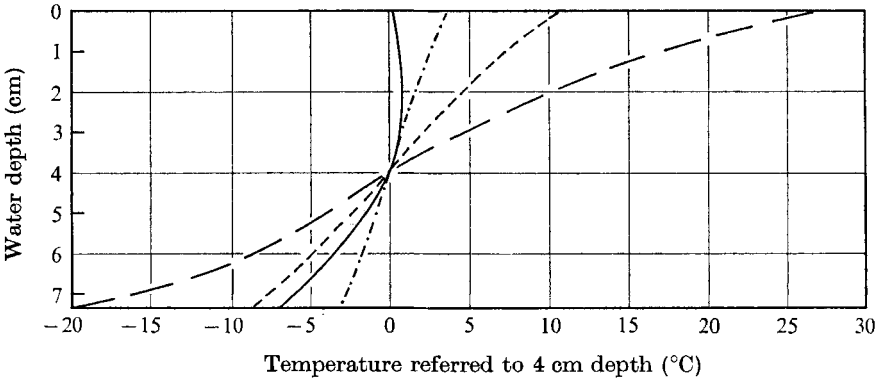

FIGURE 2. Temperature *vs.* depth profiles. ——, profile 1; – – –, profile 3; ——, profile 4; –·–·, profile 6.

Figure 2 shows four different profiles of temperature *vs.* depth established by using various combinations of electrical current through the thermo-electric devices (not all shown in figure 1). For example, profile 2 was established by passing 10 A with polarity to cool the bottom and 10 A with polarity to heat the top. Profile 3 required 5 A cooling current on the bottom and 5 A heating on top. Profile 6 was established with zero bottom current and 2·5 A heating at the top. Profile 4 required 10 A bottom cooling and zero top current. In this last case there was slight cooling at the top because the constant-temperature water circulating through the upper water jackets was somewhat cooler than the ambient temperature. The cooling was by conduction through the structure of the thermo-electric devices attached to the upper copper strip. It took about 2 h after the start of current flow for the temperature profiles to stabilize at the values shown in figure 2. (Profiles 2 and 5 are omitted from this report.)

Figure 3 shows the four temperature profiles of figure 2 converted to four corresponding density profiles. The conversion was made using handbook data relating pure water temperature with density, together with a reference temperature for each temperature profile curve. The horizontal scale is in the σ_t density unit commonly used by oceanographers (Sverdrup *et al.* 1942). In this case $\sigma_t = (\rho - 1) \times 10^3$, where ρ is the water density in g/cm^3. The negative abscissa values are density expressed in parts per thousand, and density increases from left to right.

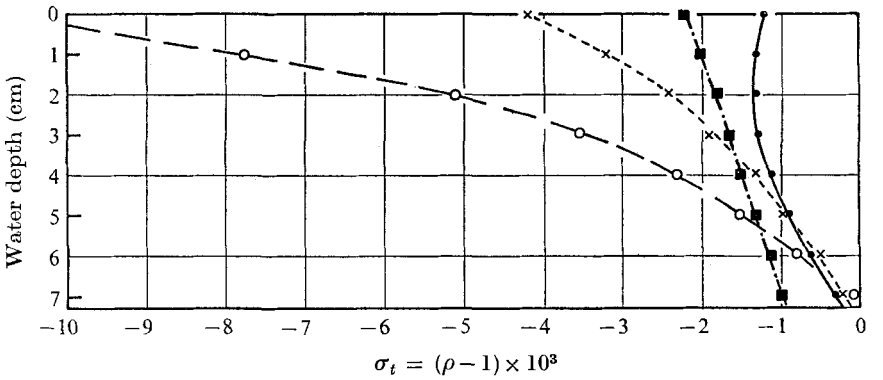

FIGURE 3. Density (σ_t) *vs.* depth profiles. ○—○, profile 1; × - - ×, profile 3; ●—●, profile 4; ■-·-■, profile 6.

For density profiles 1 and 3 the density gradient with respect to water depth, $d\sigma_t/dz$, is greater at the top and decreases with depth. For profile 6 the density gradient is very nearly constant. Profile 4 shows a region where density decreases with depth near the top, then a region of approximately zero gradient which changes to a region of approximately constant-density gradient near the bottom.

A prominent feature near the centre of figure 1 is a 1·3 cm diameter device which is a non-rotatable mixer. A lever system connects it with a drive mechanism that will move the mixer forward and backward about ± 1 cm ten times in about 2–2·5 sec on demand. This vigorous back-and-forth movement will generate a pulse of turbulence which will first expand and then collapse vertically (Wu 1969; Schooley 1968). The restoring force is gravity acting on ρ and $d\sigma_t/dz$. It is the resulting change in the temperature structure with time after mixing which makes it comparatively simple to study the internal wave structure for the various temperature or density profiles of figures 2 and 3.

Figure 1 shows a small thermistor bead projecting about 2·5 mm through a small hole in the upper copper strip, directly above the mixer. The thermistor was connected to a calibrated recording system which yielded a time record of the temperature at this point before, during and after mixing. Since the thermistor was used in a manner which was relatively insensitive to velocity it recorded temperature changes due to vertical motion of the stratified water at the point of measurement. A second thermistor bead is also shown projecting through a hole in the copper strip near the centre of the right half of figure 1. Although not visible, there are small holes for inserting thermistors at four different places along the copper strip on each side of the centre-line (℄).

Figure 4 shows the results of experiments. In figure 4 (*a*) the time scale proceeds downward for 40 sec after the start of mixing and the horizontal scale measures distance from zero at the centre of the upper copper strip (℄) and proceeds 15 cm to the right. The curves represent smoothed processed data from several experiments using profile 1. The long-dashed curves are regions where the thermistor recording system showed positive maximum readings, compared to the situation before mixing. The short-dashed curves show regions of negative maximum temperature readings. The solid lines are the regions where the temperature was the same as before mixing.

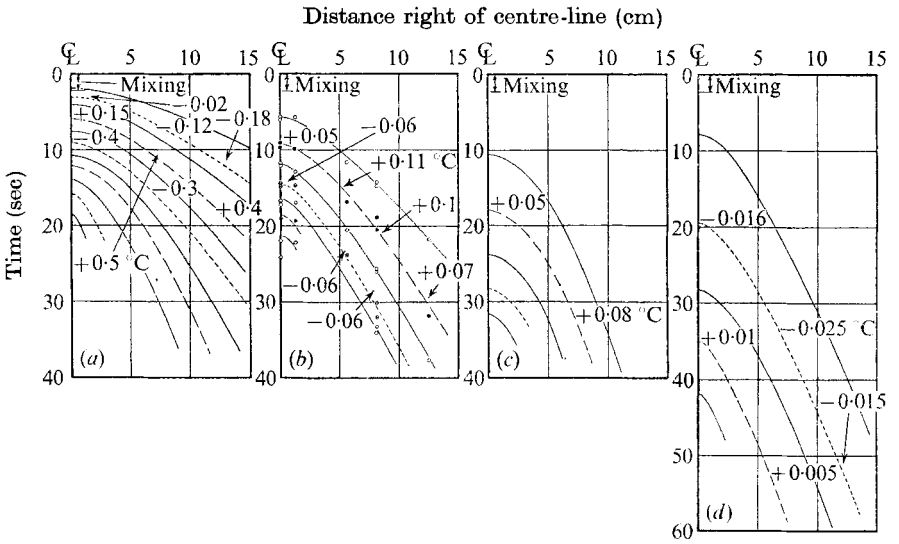

FIGURE 4. Experimentally determined constant phase lines. (*a*) Temperature profile 1, (*b*) temperature profile 3, (*c*) temperature profile 6, (*d*) temperature profile 4.

The pattern revealed by figure 4 (*a*) is that of a series of internal waves initiated by a pulse of turbulence caused by the 1·3 cm diameter mixer, 4·5 cm below the upper water boundary and on the centre-line of the experimental cell. To save space, only the right half of the internal wave pattern is shown. A similar symmetrical set of internal waves also occurs to the left. At various places in the negative and positive regions of the internal waves the approximate amplitudes of the temperature deviations are shown. Since the water near the top was warmer than that below, a negative temperature indicates an upward component of water flow and a positive temperature means a downward component of flow. The first convergence due to the vertical collapse caused the strong positive wave which grew from about +0·15 °C near the centre to +0·5 °C about 7·5 cm from the centre.

Internal wave absorbers were used at the right and left ends of the cell (not shown in figure 1) in an attempt to minimize end reflexions. However absorption was not complete and quantitative data was not attempted when it was thought that reflexion interference might be present.

Figure 4 (*b*) is the same as figure 4 (*a*) except that it is for profile 3 instead of

profile 1. In this case the figure shows experimental points to give an example of the amount and consistency of the original data. The temperature gradient is less in figure 4(*b*) than in figure 4(*a*) and for this reason the initial negative wave was too small to be measured. The first wave in figure 4(*b*) is due to the first convergence caused by the vertical collapse of the initial turbulent divergence. The internal waves for the profile 3 condition (figure 4*b*) are shown to travel more slowly than for the stronger temperature gradient profile 1 (figure 4*a*).

Figure 4(*c*) is for the weak and quite linear profile 6. A weak temperature gradient makes temperature variations due to the internal waves more difficult to measure. However, enough data are available to show that the internal wave speed is still less than for the previously discussed stronger gradients.

Figure 4(*d*) shows the internal waves when profile 4 was used. In this case there was a rather weak gradient at the mixer depth with an isopycnal intermediate region above. At the top the water was slightly colder above than below, but apparently not enough to induce convection. The results of the experiment show slowly travelling internal waves where the collapse of the initial turbulent pulse induces first a negative and then a positive temperature wave. This is the reverse of figures 4(*b*) and 4(*c*) and is due to the change in the sign of the gradient near the top for profile 4 compared to the case for profiles 3 and 6.

3. Theoretical analysis

In this section a theoretical model which is based on the conditions which prevailed during the experimentation is discussed. Calculations using this model have been made and are presented for comparison with the recorded data.

A number of simplifying and idealizing assumptions have been used, most of which are common to the first-order study of internal waves (e.g. Mowbray & Rarity 1967). Besides the usual assumptions of linearity, Boussinesq approximation and no molecular diffusion of those properties that define the density, the following more specialized assumptions are made: (i) Molecular viscosity is included by means of a perturbation expansion, following Dore (1968). This assumption will be dealt with more fully later. (ii) The initial disturbance, and thus the resulting flow pattern, is strictly two-dimensional. (iii) The initial velocity structure is zero. (iv) The end walls are infinitely distant. (v) The analysis, later on, is particularized to the case in which the Brunt–Väisälä frequency is independent of depth. It is unfortunate that more information was not available about the degree of mixing prior to collapse. However, it is expected that, at least over the area of the stirrer, mixing was virtually complete and any incompleteness was near the edge of the mixed region. If this were the case, it would show up in the resulting wave field mainly as a deficiency of high-order modes. It will be shown below that for the comparison with the experimental data, low-order modes are dominant (owing to geometrical coupling and viscous effects). For the present problem therefore, the simplest mathematical representation of the initial state will be used, namely a perfectly mixed circular region.

Of all these assumptions, (iii) and (v) are probably the most unlike the experimental conditions for short-term observations. Initially, and very near the

'edge' of the mixed region, all assumptions (except possibly (iv)) are expected to break down. However, this breakdown should apply mainly to very short length-scales, and since their group velocities are low and viscous damping high they are not expected to contribute materially to the flow pattern. Also, the turbulent velocity structure existing initially will be most energetic in length-scales less than the initial diameter of the mixed region and will be almost completely contained within the mixed region; thus the direct coupling between this structure and the resulting wave field will be low (especially for waves long compared with the initial diameter).

Non-linearities in the resulting wave field may be important for a short time after the beginning of collapse and near the mixed region. An upper estimate for the vertical amplitude of wave motion is $\frac{1}{5}a$ (Wu 1969), where a is the radius of the mixed region, thus the ratio of the non-linear terms in the equations of motion to a typical linear term is given by $\frac{1}{5}ak$, where k is the wave-number of the wave-field. From figure 4 and table 1 the largest value of this parameter is 0·35 (profile 1). For regions or times removed from the onset of collapse this parameter is expected to be substantially reduced (figure 7(*a*) or Wu 1969).

The position at which the measurements were taken is very near a solid boundary so there is the possibility of a substantial modification of the inviscid wave-pattern by boundary-layer effects. Also, since the Brunt–Väisälä frequency is of order 1 per sec there is the likelihood of appreciable viscous dissipation within the body of the fluid and by the walls. It was not expedient to perform a new set of experiments (the ones reported here were done some years before the theory was undertaken), so instead, these viscous effects are included in the theoretical model. To accomplish this, the perturbation scheme given by Dore will be used. It is directly applicable to the present problem and so only the results of that investigation will be used. It is thus necessary to solve only the inviscid equations and apply the viscous corrections later.

With the previously mentioned assumptions, the inviscid equations of motion are:

$$\frac{\partial u}{\partial x}+\frac{\partial w}{\partial z}=0, \tag{1}$$

$$\rho_0(z)\frac{\partial u}{\partial t}+\frac{\partial p}{\partial x}=0, \tag{2}$$

$$\rho_0(z)\frac{\partial w}{\partial t}+\frac{\partial p}{\partial z}=\rho g, \tag{3}$$

$$\frac{\partial \rho}{\partial t}+w\frac{\partial(\rho_0(z))}{\partial z}=0, \tag{4}$$

with x horizontal and perpendicular to the axis of the mixed region, z positive downwards, $\rho_0(z)$ the density profile before mixing, ρ the instantaneous difference between the total density and ρ_0, p the instantaneous difference between the total pressure and the hydrostatic head, g the acceleration of gravity, u, w the velocity components in the x, z plane, and t the time. The boundary conditions are

$$w=0 \quad \text{at} \quad z=0, D \quad \text{for all time}, \tag{5}$$

$$w \text{ remains bounded as } \quad x\to\pm\infty. \tag{6}$$

The initial conditions are

$$p, u, w = 0 \quad \text{for all} \quad x, z \tag{7}$$

and

$$\rho = \rho_0(z) f(x, z). \tag{8}$$

The problem is amenable to treatment by a one-sided Fourier transform in time. Thus, if

$$\overline{w} = \int_0^\infty e^{-i\omega t} w(t)\, dt \tag{9}$$

(and similar representations for all the other dependent variables), equations (1) to (4) and (8) reduce to the following equation (using the Boussinesq approximation):

$$\frac{\partial^2 \overline{w}}{\partial z^2} + \left(1 - \frac{N^2}{\omega^2}\right) \frac{\partial^2 \overline{w}}{\partial x^2} = -\frac{g}{\omega^2} \frac{\partial^2 f}{\partial x^2}, \tag{10}$$

where

$$N(z) = \left(\frac{g}{\rho_0} \frac{d\rho_0}{dz}\right)^{\frac{1}{2}}$$

is the Brunt–Väisälä frequency.

To reduce the problem further, let

$$\overline{w} = \sum_n \phi_n(z) F_n(x), \tag{11}$$

where $\phi_n(z)$ is an eigenfunction from an orthonormal set defined by

$$\frac{d^2 \phi_n}{dz^2} + \alpha_n^2 \left(\frac{N^2}{\omega^2} - 1\right) \phi_n = 0 \quad (\phi_n(z) = 0 \quad \text{at} \quad z = 0, D) \tag{12}$$

and thus

$$\frac{d^2 F_n}{dx^2} + \alpha_n^2 F_n = \frac{g}{\omega^2} \int_0^D \phi_n(z) \frac{\partial^2 f}{\partial x^2} dz \equiv \frac{d^2 I}{dx^2}. \tag{13}$$

Since I is a direct representation of the buoyancy at time zero it must vanish outside the initial mixed region. It is also necessary that $\phi_n(z)$ be the nth member of a complete set; otherwise an integral term (representing a continuous distribution of modes) is required on the right-hand side of (11). It is shown by Courant & Hilbert (1953) that $\phi_n(z)$ is complete if $\overline{w}$ possesses continuous first and piecewise continuous second derivations (in z), i.e. from (10), if N (or f) is at worst piecewise continuous in z. Thus the solution of (13) satisfying (6) is

$$F_n(x) = I - \tfrac{1}{2} i \alpha_n \left(e^{i\alpha_n x} \int_x^\infty e^{-i\alpha_n \eta} I(\eta)\, d\eta + e^{-i\alpha_n x} \int_{-\infty}^x e^{i\alpha_n \eta} I(\eta)\, d\eta \right). \tag{14}$$

Let the initial mixed region be symmetric in x with its midpoint at $(0, z_0)$ and its maximum horizontal extent given by $2a$. Then the total wave field exterior to the initial mixed region can be obtained from

$$F_n(x) = -i\alpha_n e^{-i\alpha_n |x|} \int_0^a \cos(\alpha_n \eta) I(\eta)\, d\eta \quad (|x| > a). \tag{15}$$

Using the inverse transform to (9),

$$w = \frac{1}{2\pi} \int_{-\infty - i\epsilon}^{+\infty - i\epsilon} \sum_n \left(-i\alpha_n e^{-i\alpha_n |x| + i\omega t} \phi_n(z) \int_0^a \cos(\alpha_n \eta) I(\eta)\, d\eta \right) d\omega, \tag{16}$$

where ϵ is chosen to ensure that the integration is below the singularities of the integrand.

The initial buoyancy function $I(x)$ is given by

$$I = \frac{g}{\omega^2}\int_0^D f(x,z)\,\phi_n(z)\,dz,$$

where, for a circular, completely mixed region,

$$f(x,z) = (\rho_0(z_1)/\rho_0(z) - 1)\,H(x+a)\,H(a-x)\,H(z-z_0+(a^2-x^2)^{\frac{1}{2}})\,H(z_0-z+(a^2-x^2)^{\frac{1}{2}}). \tag{17}$$

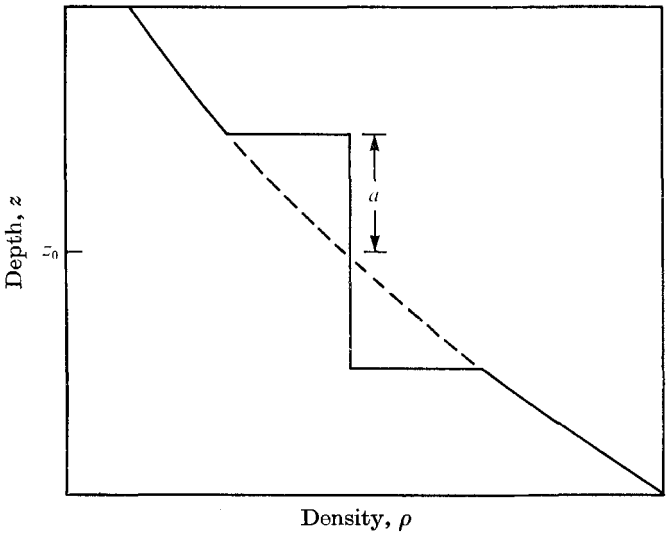

FIGURE 5. Theoretical model of the initial density *vs.* depth through the centre-line of the mixed region.

Here z_0 is the depth of the centre of the region, H is the Heaviside unit function and $\rho_0(z_1)$ is the density of the mixed region (see figure 5).

In terms of the Brunt–Väisälä frequency,

$$\frac{\rho_0(z_1)}{\rho_0(z)} = \exp\left\{-\int_{z_1}^{z} N^2(z)/g\,dz\right\},$$

or, using the Boussinesq approximation,

$$\frac{\rho_0(z_1)}{\rho_0(z)} = 1 - \int_{z_1}^{z}\frac{N^2(z)}{g}\,dz. \tag{18}$$

Thus,
$$I = \frac{H(x+a)\,H(a-x)}{\omega^2}\int_{z_0-(a^2-x^2)^{\frac{1}{2}}}^{z_0+(a^2-x^2)^{\frac{1}{2}}}\phi_n(x)\int_{z_1}^{z} N^2(z')\,dz'\,dz. \tag{19}$$

The general solution represented by equations (19), (16) and (12) will now be restricted to the present experimental case. The density profiles shown in figure 3 indicate that the approximation $N^2 =$ constant should provide most of the pertinent features of the internal wave field. With $N = N_0$ and $z_1 = z_0$,

$$\phi_n(z) = \frac{2^{\frac{1}{2}}\sin(n\pi z/D)}{\{D(N_0^2/\omega^2-1)\}^{\frac{1}{2}}}, \tag{20}$$

$$\alpha_n = \frac{n\pi}{D\{N_0^2/\omega^2-1\}^{\frac{1}{2}}}, \tag{21}$$

and

$$\int_0^a \cos(\alpha_n \eta) I(\eta) d\eta = -\frac{a^2}{n}\left[2D\left(\frac{N_0^2}{\omega^2}-1\right)\right]^{\frac{1}{2}} \cos\left(\frac{n\pi z_0}{D}\right) J_2\left(\frac{an\pi}{D(1-\omega^2/N_0^2)^{\frac{1}{2}}}\right), \quad (22)$$

where J_2 is the Bessel function of second order. Therefore, interchanging the order of integration and summation in (16) (which is permissible by the rules governing Fourier series representing generalized functions),

$$w = ia^2 \sum_{n=1}^{\infty} \frac{\sin(n\pi z/D)\cos(n\pi z_0/D)}{n\pi} \int_{-\infty-i\epsilon}^{+\infty-i\epsilon} \alpha_n J_2\left(\frac{an\pi}{D(1-\omega^2/N_0^2)^{\frac{1}{2}}}\right) e^{i\omega t - i|x|\alpha_n} d\omega. \quad (23)$$

This expression can be simplified by contour integration. For $t > 0$ it can be shown that there is no modification to the value of this integral if the integration path is closed by an infinite semicircle in the upper half plane. For $t < 0$ the lower half plane can be used. Thus the value of w arises only from integration around the singularities $\omega = \pm N_0$ (in α_n). Since these are branch points a cut is necessary and it is convenient to take the cut along the real ω axis between $\pm N_0$. Integration around the branch points produces no contribution, so (23) reduces to an integration along the bottom of the cut from $-N_0$ to $+N_0$ and an integration along the top in the opposite direction. In appendix A it is shown that

$$d(\alpha_n^2)/d(\omega^2) > 0$$

near the real ω axis and that this condition together with the condition of boundedness at large $|x|$ leads to the restriction that the real parts of ω and α_n must have the same sign for ω slightly below the real axis. Therefore, on the bottom of the cut $\alpha_n \gtrless 0$ for $\omega \gtrless 0$ and on top $\alpha_n \lessgtr 0$ for $\omega \gtrless 0$.

Finally, with $\epsilon = 0$,

$$w = -\frac{4a^2}{D} \sum_{n=1}^{\infty} \sin\left(\frac{n\pi z}{D}\right) \cos\left(\frac{n\pi z_0}{D}\right) \int_0^{N_0} \frac{J_2(an\pi/D(1-\omega^2/N_0^2)^{\frac{1}{2}})}{(N_0^2/\omega^2-1)^{\frac{1}{2}}} \times \sin\omega t \cos\left(\frac{n\pi x}{D(N_0^2/\omega^2-1)^{\frac{1}{2}}}\right) d\omega. \quad (24)$$

For $t < 0$ there are no singularities. Thus

$$w = 0 \quad \text{for} \quad t < 0. \quad (25)$$

Using the linearity assumption and the transformation $\omega = N_0 \cos\theta$,† the amplitude $\zeta (= \int w\, dt)$ is given by

$$\underset{\substack{|x|\gtrless a \\ t>0}}{\zeta} = \frac{4a^2}{D} \sum_{n=1}^{\infty} \sin\left(\frac{n\pi z}{D}\right) \cos\left(\frac{n\pi z_0}{D}\right) \int_0^{\frac{1}{2}\pi} J_2\left(\frac{an\pi}{D\sin\theta}\right) \cos(N_0 t\cos\theta) \cos\left(\frac{n\pi x}{D\tan\theta}\right) d\theta. \quad (26)$$

This represents the inviscid solution.

† It can easily be seen that to this approximation θ represents the angle between the vertical and the local lines of constant phase or 'crest' lines of that particular frequency component. If $\theta = 0$ the lines of constant phase are vertical and if $\theta = \frac{1}{2}\pi$ the lines are horizontal.

To incorporate the most important effects of viscosity it is necessary to return to equation (16) and perturb the frequency ω in $e^{i\omega t}$ and to modify ζ to allow for boundary-layer effects. The resulting equations are obtained in appendix B. Some general characteristics of the form that the internal wave pattern possesses will now be outlined.

The finite depth of the model has resolved the pattern into an infinite series of modes. (This situation remains true for an infinite depth if N is piecewise continuous and $\to 0$ as $z \to \infty$). The horizontal inviscid group velocity of the nth mode, Cg_n, is given by

$$Cg_n = \frac{d\omega}{d\alpha_n} = \frac{N_0 D n^2 \pi^2}{(n^2\pi^2 + D^2\alpha_n^2)^{\frac{3}{2}}} = \frac{N_0 D}{n\pi} \sin^3\theta. \tag{27a}$$

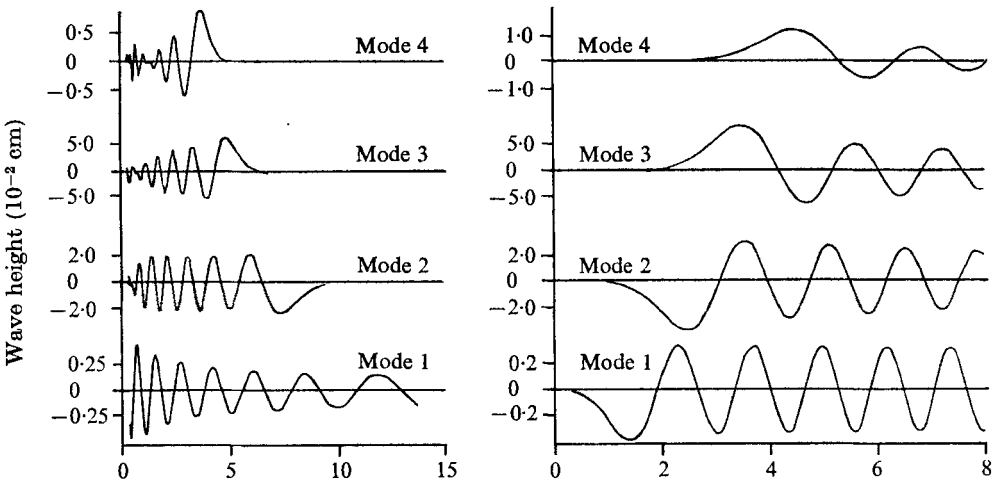

(*a*) Distance in units of D

(*b*) Time in units of the Brunt–Väisälä period

FIGURE 6. Illustration of the mode structure of an inviscid internal wave field. The modes have been separated to show comparative features: (*a*) wave height at an instant as a function of distance from the centre-line, $N_0 t = 50$; (*b*) wave height at one particular point as a function of time from beginning of the collapse, $x/D = 2$. (For this example: $N_0 = 0{\cdot}25$ sec^{-1}, $a = 2{\cdot}05$ cm, $D = 7{\cdot}3$ cm, $z = 0{\cdot}3$ cm, $z_0 = 4{\cdot}5$ cm and viscosity $= 0$.)

Also, the horizontal phase velocity C_n is

$$C_n = \frac{\omega}{\alpha_n} = \frac{N_0 D}{n\pi} \sin\theta. \tag{27b}$$

The maximum group velocity $N_0 D/\pi$ (which is the same as the maximum phase velocity) increases directly with N_0. This is in accordance with the experimental observation that the wave velocity increases as the density gradient (or N_0) increases. Also, the horizontal extent of the wave-pattern for each mode is limited at any instant and at higher mode numbers the limitation appears nearer the centre-line of the mixed region. Within this horizontal limitation a wave-field stretching back to the centre-line can exist.

A stationary phase reduction of equation (26) (with N_0 large) indicates that a

stationary phase contribution exists for every point within this possible wave-field. Equation (27) gives the value of θ at which the phase of equation (26) is stationary for $|x|/t = Cg_n$. As $|x| \to 0$, $\theta \to 0$, the horizontal wave-number $n\pi/D \tan\theta \to \infty$ and $\omega \to N_0$. Therefore each mode gives rise not to a localized group of waves but to a field extending from the centre-line to the limiting extent for that particular time. The wavelength within the field increases from zero to ∞ over this same region. Figure 6 (*a*) illustrates this behaviour.

As a function of time at a given position the wave-pattern is essentially zero until the most rapid ($n = 1$) mode arrives (at t, say) and exhibits a continuing oscillation in time with a frequency rising from zero asymptotically at N_0. At $2t$ the second mode arrives and exhibits a similar behaviour in frequency and so on for all the modes. This is shown in figure 6 (*b*).

If only one mode is present the wave-field will exhibit dispersion characteristics pertaining to that mode. If more than one mode is dominant, as is true for the example used in figure 6, interference effects will also be apparent.

The damping effects of viscosity are most pronounced for high modes and high frequencies ($\theta \approx 0$). Waves nearest the centre-line at any given instant or waves appearing at later times at any given position are reduced the most. The local frequency is also reduced by viscosity.

All these general characteristics are in agreement with the measured patterns shown in figure 4 even though these do not satisfy the condition $N_0 t \to \infty$. The only major exceptions occur in the vicinity of the initial mixed region. In figure 4 (*a*) the distance between zeros along the 10 sec line increases away from the centre-line. The same behaviour can be seen in 4 (*b*) along the 20 sec line. Also, the time between zeros along the 5 cm line in figure 4 (*b*) decreases towards later times (although in figure 4 (*a*) the bottom curves indicate a slight opposite tendency). However, not only may asymptotic arguments be expected to fail there and viscous effects dominate, but the region $|x| < a$ (for all z) has been previously excluded from the domain of applicability of the solution. It is also apparent from the measurements that a simple wave field exists, implying the presence of only a few modes.

To accomplish a direct comparison of the theory with experimental results the temperature excursion from ambient was calculated using $\Delta T = \zeta(dT/dz)$ evaluated at z, the depth of the thermistor bead, for each profile shown. The values used in equation (B 3) are listed in table 1. Each of these values was obtained from the experimental data. The listed values of N_0 are the averages of the Brunt–Väisälä frequency over the total depth of the tank for each profile. In each case the average was calculated from an exponential curve of $N(z)$ fitted with a least-square technique to individual values of N obtained from figure 3. The accuracy of N_0 is estimated at $\pm 10\%$. Maximum vertical expansion of the turbulent pulses was determined by dye and cinematography techniques (Schooley 1968). One-half the expansion determined a to an accuracy of about $\pm 10\%$.

The values of viscosity listed were obtained from standard handbook tables and pertain to the measured values of temperatures: $\bar{\nu}$ corresponds to an average throughout the tank, ν corresponds to the value at the thermistor depth.

It was not expected that mode 1 would be important since it represents fluid travelling all up or all down in a given column. Instead the initial buoyancy pattern is such that it would couple well into modes which represent a downward velocity above z_0 and an upward velocity below z_0. If z were exactly half of D, the flow would therefore be mode 2 with contributions from the other even ordered modes because of the initially round shape. In fact, in (26) all odd modes do

Profile	a (cm)	N_0 (sec^{-1})	dT/dz (°C/cm)	ν (cgs)	z (cm)
1	2·00	1·19	11·1	0·006	0·250
3	2·05	0·68	3·81	0·009	0·300
6	2·35	0·41	1·18	0·010	0·325

TABLE 1. $z_0 = 4{\cdot}5$ cm, $D = 7{\cdot}3$ cm, $\bar{v} = 0{\cdot}01$ cm/sec^2

vanish under this condition. With the present ratio of $z_0/D = 0{\cdot}616$ it is expected that mode 3 will also be important since the eigenfunction for $n = 3$ has a zero at $z/D = \frac{2}{3}$. A large contribution from modes 2 and 3 is apparent in the example shown in figure 6. For the calculations used in the comparison with the measured data enough modes were included in the summation to ensure stability of one part in 10^3 in the final value of ζ. The necessary number of modes ranged from 4 at large $|x|$ and ζ to 30 at small $|x|$ and ζ. Typically, mode 2 was dominant with some substantial contributions from modes 3 and 5.

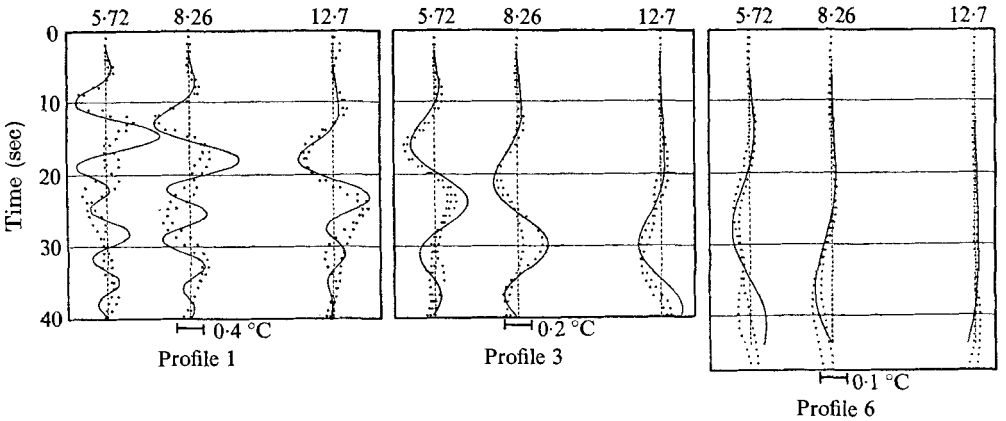

FIGURE 7. Temperature excursion *vs.* time. —, theoretical curves; ..., experimental values. The position of each line is in scale with its distance from the centre-line. The distances in centimetres are shown above each line.

The comparison is shown in figure 7. The dotted lines represent measured data, the solid lines are the theoretical curves. At least two sets of measured data were obtained for each profile. The time origin for the calculated curves has had one adjustment for each profile to provide a visual 'best' fit to the measured curves. This is considered permissible because the instant when collapse began is not known experimentally. This is because the concept itself is an idealization: collapse can occur during the entire stirring and turbulent expansion

interval. Also, a small change in N_0 or any variation in the Brunt–Väisälä frequency with depth will affect the velocity of the waves without appreciably affecting their amplitudes, thus effectively producing a difference between experimental and theoretical time origins. The time shifts actually used are 1·6, 1·6 and 4·0 sec for profiles 1, 3 and 6 respectively. As in figure 4, the time origin refers to the instant the mixer was turned on. For each curve the distance in centimetres from the centre-line to the base-line at which those measurements were obtained is shown by the number at the top of each figure. The excursions from the base-line represent the temperature deviations from ambient and are scaled at the bottom of each figure. For profile 1 the fit is good only for the first wave. After that the theoretical curves predict more waves than are experimentally found

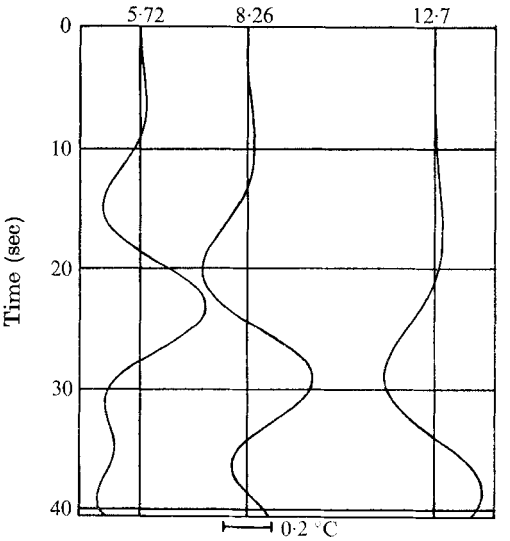

FIGURE 8. Calculated temperature excursions for profile 3 with zero viscosity. The number above each line is its horizontal distance from the centre-line in centimetres.

(except for the measurements at 12·7 cm). Nevertheless the amplitudes of the theoretical excursions are very similar to the measurements. For profiles 3 and 6 the measurements and the theoretical curves are in reasonably good agreement.

The inviscid solution for profile 3 is shown in figure 8. It can be seen that for this scale of motion viscosity is indeed important and over the recorded time interval reduces the amplitude of the wave typically by a factor of two. The degree of matching between (B 1) and (22) was tested by sample calculations on profiles 1 and 6. Equation (B 1) was used in (B 3) with $\nu = 0$ ($\bar{\nu} \neq 0$) and compared with the results for ϕ_n in place of ψ_n in (B 3). Both functions gave the same results with differences of about 5 %.

Equation (26) indicates that the wave amplitude is fairly strongly dependent on the radius of the initial mixed region. If $a/D \ll 1$,

$$J_2(an\pi/D\sin\theta) \approx (an\pi/D\sin\theta)^2 \times \tfrac{1}{8}$$

for low mode numbers and low frequencies. In this case $\zeta \propto a^4$. If the mode number of the dominant waves is large enough or the frequency of the dominant waves is small enough, or if $a/D = O(1)$, $J_2(an\pi/D \sin\theta)$ is essentially independent of a and so $\zeta \propto a^2$.

4. Conclusions

It has been shown that the internal wave amplitudes generated by the two-dimensional collapse of an initially turbulent region can be predicted (at least near a boundary) using a highly idealized linear model. The accuracy of the prediction is only loosely determined but for these measurements it is approximately the same as the experimental scatter. The discrepancy in time of arrival of the waves between theory and experiment, as is indicated by the adjustment in the time origin of the theoretical values, is believed to be due mainly to two effects: variations in the Brunt–Väisälä frequency from the assumed constant profile and non-zero mixing time.

Appendix A

The eigenvalue α_n and the eigenfunction $\phi_n(z)$ are defined by

$$\frac{d^2\phi_n}{dz^2} + \alpha_n^2 \left(\frac{N^2(z)}{\omega^2} - 1\right) \phi_n = 0 \quad (\phi_n(z) = 0 \quad \text{at} \quad z = 0, D) \tag{A 1}$$

and

$$\int_0^D \left(\frac{N^2}{\omega^2} - 1\right) |\phi_n|^2 dz = 1. \tag{A 2}$$

(Equation (A 1) is the same as (12) in the main part of the paper.) Differentiate (A 1) by ω^2 and set $\partial\phi_n/\partial\omega^2 = \psi_n$,

$$\frac{d^2\psi_n}{dz^2} + \alpha_n^2 \left(\frac{N^2}{\omega^2} - 1\right) \psi_n + \frac{d\alpha_n^2}{d\omega^2} \left(\frac{N^2}{\omega^2} - 1\right) \phi_n - \frac{\alpha_n^2 N^2}{\omega^4} \phi_n = 0. \tag{A 3}$$

Multiply (A 3) by ϕ_n^*, the complex conjugate of ϕ_n, and integrate over all z, then

$$-\int_0^D \left(\frac{d\phi_n^*}{dz}\frac{d\psi_n}{dz}\right) dz + \alpha_n^2 \int_0^D \left(\frac{N^2}{\omega^2} - 1\right) \psi_n \phi_n^* dz + \frac{d\alpha_n^2}{d\omega^2} = \frac{\alpha_n^2}{\omega^4} \int_0^D N^2 |\phi_n|^2 dz. \tag{A 4}$$

Take the complex conjugate of (A 1), multiply by ψ_n and integrate over all ω. Since ω is real α_n is real,

$$-\int_0^D \left(\frac{d\psi_n}{dz}\frac{d\phi_n^*}{dz}\right) dz + \alpha_n^2 \int_0^D \left(\frac{N^2}{\omega^2} - 1\right) \phi_n^* \psi_n dz = 0,$$

and, from (A 4),

$$\frac{d\alpha_n^2}{d\omega^2} = \frac{\alpha_n^2}{\omega^4} \int_0^D N^2 |\phi_n|^2 dz. \tag{A 5}$$

Therefore $(d\alpha_n^2)/d\omega^2 > 0$ and, in fact, since

$$\int_0^D \frac{N^2}{\omega^2} |\phi_n|^2 dz = 1 + \int_0^D |\phi_n|^2 dz$$

(by A 3), which is greater than 1, $d\alpha_n^2/d\omega^2 > \alpha_n^2/\omega^2$. This shows that the horizontal group velocity is always less than the horizontal phase velocity.

Let $\omega = \omega_r - i\epsilon$ and $\alpha_n = \alpha_{nr} + i\delta$. Then for small ϵ,

$$\delta = -\epsilon \frac{\omega_r}{\alpha_{nr}} \left(\frac{d\alpha_n^2}{d\omega^2}\right)_{\epsilon=0}.$$

However, in order that $F(x)$ remains bounded as $x \to \pm\infty$, δ must be negative (equation 14). Therefore, since $\epsilon > 0$ (equation 16) and $d\alpha_n^2/d\omega^2 > 0$, ω_r and α_{nr} must have the same sign.

Appendix B

Using the perturbation expansion set up by Dore, equation (20) represents the inviscid outer solution to the problem. The lowest order 'inner' solution, near the top boundary, is given by

$$\psi_n = \frac{2^{\frac{1}{2}}}{\{D(N_0^2/\omega^2 - 1)\}^{\frac{1}{2}}} \left\{ \frac{n\pi z}{D} + \frac{n\pi}{D}\left(\frac{\nu}{2\omega}\right)^{\frac{1}{2}} \left[1 - 2^{\frac{1}{2}} e^{-z(\omega/2\nu)^{\frac{1}{2}}} \cos\left(z(\omega/2\nu)^{\frac{1}{2}} + \tfrac{1}{4}\pi\right) \right.\right.$$
$$\left.\left. + i[1 - 2^{\frac{1}{2}} e^{-z(\omega/2\nu)^{\frac{1}{2}}} \cos\left(z(\omega/2\nu)^{\frac{1}{2}} - \tfrac{1}{4}\pi\right)] \right] \right\}, \quad \text{(B 1)}$$

where ν is the local kinematic viscosity. It is also shown by Dore that the frequency in equation (16) must be replaced by a perturbed frequency ω_p. To second order in the expansion

$$\omega_p = \left(|\omega| - \left(1 - \frac{\omega^2}{N_0^2}\right)\left(\frac{2|\omega|\bar{\nu}}{D^2}\right)^{\frac{1}{2}} \right) \operatorname{sgn}(\omega) - i\left\{ \left(1 - \frac{\omega^2}{N_0^2}\right)\left(\frac{2|\omega|\nu}{D^2}\right)^{\frac{1}{2}} \right.$$
$$\left. + \frac{\bar{\nu}}{D^2}\left[\frac{n^2\pi^2}{2(1 - \omega^2/N_0^2)} + \frac{6\omega^2}{N_0^2}\left(1 - \frac{\omega^2}{N_0^2}\right) - 2\left(1 - \frac{\omega^2}{N_0^2}\right)^2 \right] \right\}, \quad \text{(B 2)}$$

where $\bar{\nu}$ is the average of the kinematic viscosities at $z = 0$ and $z = D$.

If (B 1) and (B 2) are substituted in (23) and the previously outlined steps are taken, an equation for ζ analogous to (26) is obtained. In a simplified form

$$\zeta = \frac{2}{\pi} \sum_{n=1}^{\infty} \cos\left(\frac{n\pi z_0}{D}\right) \int_0^{N_0} \frac{\alpha_n}{\omega_r} J_2\left(\frac{an\pi}{D(1 - \omega_r^2/N_0^2)^{\frac{1}{2}}}\right) e^{-\omega_i t}$$
$$\times [\psi_r \cos(\omega_r t)\cos(\alpha_n x) + \psi_i \sin(\omega_r t)\cos(\alpha_n x)]\, d\omega, \quad \text{(B 3)}$$

where $\psi_n = \psi_r + i\psi_i$ and $\omega_p = \omega_r(\omega) - i\omega_i(\omega)$.

REFERENCES

COURANT, R. & HILBERT, D. 1953 *Methods of Mathematical Physics*, vol. 1. Interscience.

DORE, B. D. 1968 Oscillations in a non-homogeneous viscous liquid. *Tellus*, **20** (3), 514.

LIGHTHILL, M. J. 1967 On waves generated in dispersive systems by travelling forcing effects, with applications to the dynamics of rotating fluids. *J. Fluid Mech.* **27**, 725–752.

MILES, J. W. 1970 Internal waves generated by a horizontally moving source. *J. Geophys. Fluid Dynamics*, **2**, 63–87.

MOWBRAY, D. E. & RARITY, B. S. H. 1967 A theoretical and experimental investigation of the phase configuration of internal waves of small amplitude in a density stratified liquid. *J. Fluid Mech.* **28**, 1–16.

PIERCE, A. D. & POSEY, J. W. 1970 Theoretical prediction of acoustic-gravity pressure waveforms generated by large explosions in the atmosphere. AFCRL 70-0134, Dept. of Mech. Engr. M.I.T.

SCHOOLEY, A. 1968 Wake collapse in stratified fluid: experimental exploration of scaling characteristics. *Science*, **160**, 763–764.

SCHOOLEY, A. & STEWART, R. W. 1963 Experiments with a self-propelled body submerged in a fluid with a vertical density gradient. *J. Fluid Mech.* **15**, 83–96.

STOCKHAUSEN, P. J., CLARK, C. B. & KENNEDY, J. F. 1966 Three-dimensional momentumless wakes in density-stratified liquids. *Hydrodynamics Laboratory, M.I.T. Tech. Rep.* no. 93.

SVERDRUP, H. U., JOHNSON, M. W. & FLEMING, R. H. 1942 *The Oceans, Their Physics, Chemistry and General Biology*. Prentice-Hall.

WESSEL, W. R. 1969 Numerical study of the collapse of a perturbation in an infinite density stratified fluid. *Phys. Fluids*, **12**, 171–176.

WU, J. 1969 Mixed region collapse with internal wave generation in a density-stratified medium. *J. Fluid Mech.* **35**, 531–544.

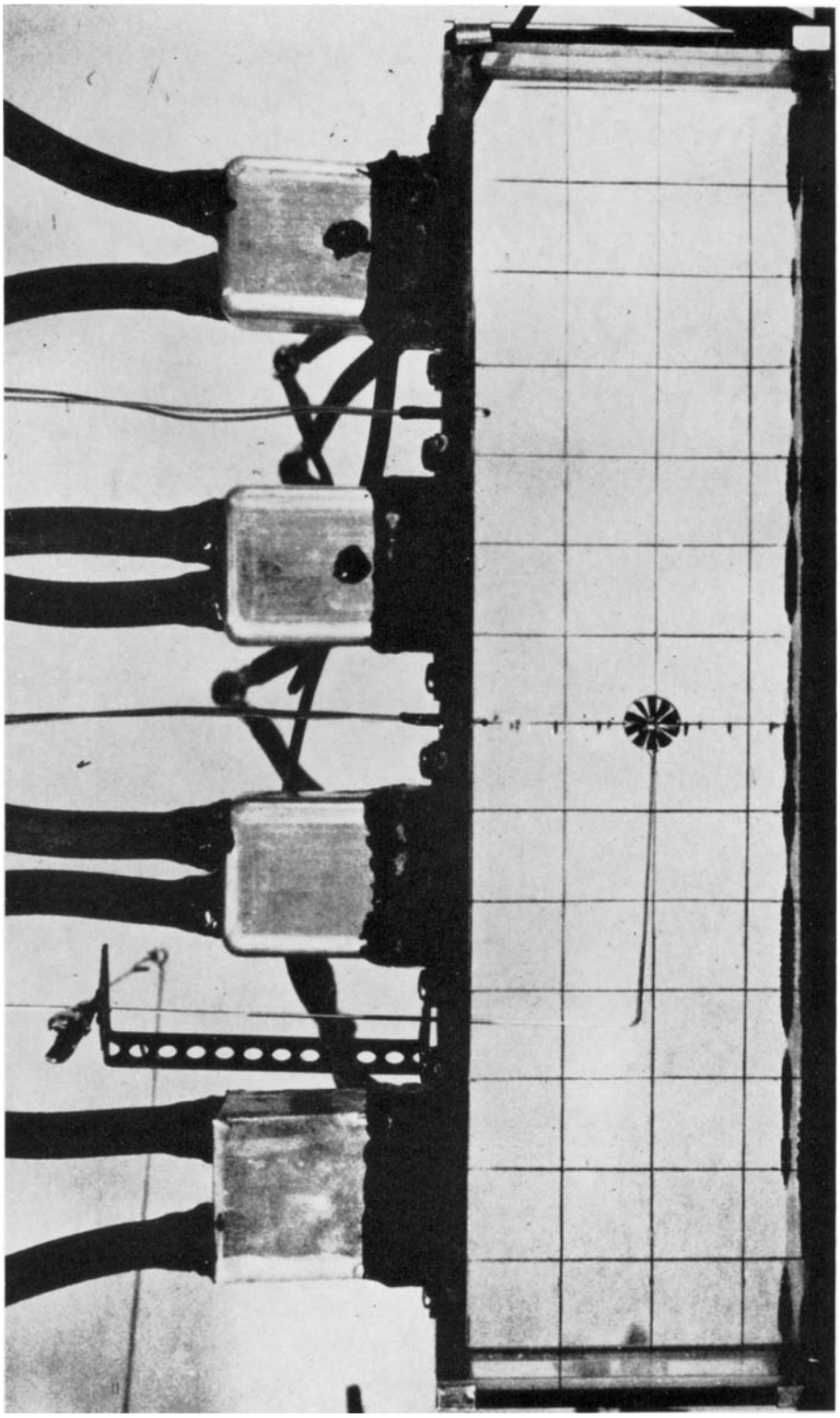

FIGURE 1. Photograph of the tank.